

Surface coating and matrix effect on the electrophoretic mobility of gold nanoparticles: a capillary electrophoresis-inductively coupled plasma mass spectrometry study

Haiou Qu¹ · Sean W. Linder¹ · Thilak K. Mudalige¹

Received: 31 August 2016 / Revised: 20 September 2016 / Accepted: 5 October 2016 / Published online: 25 October 2016
© Springer-Verlag Berlin Heidelberg (outside the USA) 2016

Abstract Capillary electrophoresis (CE) is considered as a versatile technique in the size-based separation and speciation of nanomaterials. The electrophoretic mobility is determined by charge and size of an analyte which are affected by the surface composition of nanomaterials. Size-dependent differential electrophoretic mobility is used as a mechanism for size-based separation of nanoparticles. Understanding the effect of surface chemistry on the electrophoretic mobility of nanomaterials in CE is critical in obtaining accurate results in retention-based size calculation. A suite of gold nanoparticles (NPs) varied in sizes with different coatings, including citric acid (CA), lipoic acid (LA), tannic acid (TA), polyvinylpyrrolidone (PVP), polyethylene glycol (PEG), branched polyethyleneimine (BPEI), and bovine serum albumin (BSA), were selected to evaluate their impact to the migration pattern of gold NPs. Additionally, surface-coated gold NPs dispersed in Suwannee River humic acid (SRHA) solution and fetal bovine serum (FBS) were used to investigate the matrix effect. It was found that the correlation between NP size and relative electrophoretic mobility is highly dependent on the capping agents. The matrix component in the SRHA solution only exhibited limited influence to the migration of NPs while electrophoretic behaviors were drastically altered in the presence of FBS matrix.

Keywords Capillary electrophoresis · Gold nanoparticles · Surface coating · Matrix effect

Introduction

The recent developments of nanotechnology and their application in consumer products have raised concerns about the safe use of nanomaterials [1]. Although the chemical composition of nanomaterials may not be significantly different from bulk materials, a series of physicochemical properties of nanomaterials and their interactions with the biological systems are dramatically changed due to the reduced size [2]. Currently, risk assessment of a material is generally based on its chemical composition while the physical properties are often ignored [3]. Consequently, it may generate caveats when we try to rely on existing knowledge of a material to perform risk assessment of a nanomaterial which has the same chemical composition of the bulk ones. A comprehensive characterization is needed to acquire inclusive information of nanomaterials.

For nanomaterial characterization, size is one of the most crucial metrics because it determines the physicochemical properties of a nanomaterial and their adsorption, distribution, metabolism, and excretion in the biological systems [4, 5]. Therefore, many techniques such as dynamic light scattering (DLS), electron microscopy, and spectroscopy methods have been developed to obtain insightful characteristics of nanomaterials [6–8]. Many of these techniques, however, have encountered different levels of difficulties when dealing with multi-model systems (i.e., highly polydispersed nanomaterial). The results are either biased towards the size of larger particles in population or require a large amount of time and work to achieve sufficient confidence [7, 9]. Recently, characterization methods featuring tandem

Electronic supplementary material The online version of this article (doi:10.1007/s00216-016-0012-0) contains supplementary material, which is available to authorized users.

✉ Thilak K. Mudalige
Thilak.Mudalige@fda.hhs.gov

¹ Office of Regulatory Affairs, Arkansas Regional Laboratory, U.S. Food and Drug Administration, 3900 NCTR Road, Jefferson, AR 72079, USA

instruments including a separation stage (e.g., liquid chromatography) and detection step (e.g., DLS) have drawn considerable attention [10–13]. It has been demonstrated to be an effective way in handling nanomaterials with broad size distribution. In the separation stage, nanomaterials migrate at different speeds based on size-related properties and are eluted at different times. Multiple detectors that are coupled to the separation stage can then collect the elution profiles, and size-related information can be acquired [14].

A common practice in the tandem method is to use highly uniform well-characterized nanoparticles (NPs) as standards to establish a size-based calibration curve. The sizes of unknowns can be then determined by performing the measurement under identical conditions [15]. Soto-Alvaredo and his group used gold NP to identify the elution position of silver NPs using a reversed-phase liquid chromatography system [11]. Mudalige and coworkers developed an asymmetric flow field-flow fractionation coupled with inductively coupled plasma mass spectrometry (AFFFF-ICPMS) method using gold NP standards to build a calibration curve and analyze commercial dietary supplements that contain nanomaterials. Their results demonstrated that the determined sizes were well matched with TEM results [15]. Gray et al. compared AFFFF and hydrodynamic chromatography in the separation and characterization of gold NPs. They suggested that, in both methods, NP size is correlated with the retention profiles [16]. A limitation that strongly restricts the use of such an approach is the lack of NP standards. For example, the National Institute of Standards and Technology (NIST) only released three types of particle standards, which are citrate-coated gold NP with a nominal size of 10, 30, and 60 nm; polyvinylpyrrolidone-coated silver NPs with a nominal diameter of 75 nm; and polystyrene spheres with multiple choices in size [17]. In the separation stage of the tandem method, multiple physicochemical properties determine the migration speed of a NP. For example, in AFFFF, the retention of a NP can be correlated to its hydrodynamic radius [12, 18, 19]. However, NPs of different compositions may not have the same channel behavior even if their hydrodynamic size is similar [20]. This is mainly due to the differences in surface chemistry of a NP which defines its charge density, polarity, and hydrophobicity. Therefore, careful investigations are required if one type of NPs is used as a standard to characterize a different type.

Previously, we have developed a method based on capillary electrophoresis (CE) coupled with ICPMS to separate and characterize citrate-coated gold NPs [21]. It has been demonstrated to be a high-resolution technique in obtaining size-related information. The goal of this study was to investigate the surface coating and matrix effect on the migration behavior of gold NPs in CE and evaluate the applicability of developed methodology for the analysis of nanoparticle in complex matrix. Several common surface coatings were selected

due to their varied structure, molecular weight, and charge. These surface coatings include citrate acid (CA), polyvinylpyrrolidone (PVP), lipoic acid (LA), tannic acid (TA), polyethylene glycol (PEG), branched polyethyleneimine (BPEI), and bovine serum albumin (BSA). Serum and solution containing natural organic matters (NOMs) were chosen to represent the commonly encountered matrices in biological- and environmental-related studies that involve NPs. Capillary electrophoresis is well known to have a run-to-run variation in retention time due to various factors including relaxation effect in sample plug at early stage of the run [22]. To minimize the run-to-run variation, we use a nanoparticle mobility marker and calculate the relative electrophoresis mobility instead of absolute values.

Materials and methods

Materials

Cyclohexylaminoethane sulfonic acid (CHES, 99.9 %) and sodium dodecylbenzenesulfonate (SDBS, 97.5 %) were purchased from MP Biomedical (Carlsbad, CA, USA). Potassium hydroxide pellets (>85 %), nitric acid (68–70 %, Optima ultra-pure grade), BSA-lyophilized powder, and fetal bovine serum (FBS) were acquired from Fisher Scientific (Waltham, MA, USA). 2-Propanol (TraceSELECT, ≥ 99.9 %) was purchased from Sigma-Aldrich (St. Louis, MO, USA). Suwannee River humic acid (SRHA) was purchased from the International Humic Substance Society (Denver, CO, USA). All chemicals were used as received without further purification. CdSe/ZnS quantum dots (QDs) ($E_{\max} = 665$ nm) with carboxylic acid surface groups were purchased from Ocean NanoTech (Springdale, AR, USA). Before use, QDs (4 nM) were washed with deionized water and spin filtered three times to eliminate leached metal ions from QDs and other chemical residues. The purified QDs were then redispersed in water, and the solution was diluted 15-fold. CA-coated gold NPs of 5, 15, 20, 30, and 60 nm were purchased from Ted Pella (Redding, CA, USA). Gold NP suspensions (5, 15, 20, and 30 nm) stabilized by LA, TA, PEG, PVP, and BPEI were acquired from nanoComposix (San Diego, CA, USA) and stored at 4 °C in the dark. According to the manufacturer, a 5-kDa monodentate mPEG thiol is used to prepare PEG-coated gold nanoparticles. The molecular weight of PVP and BPEI ligands is 40 and 25 kDa, respectively.

BSA-coated gold NPs were prepared from CA-coated NPs [23]. Specifically, CA-coated gold NPs (approximately 50 mg kg⁻¹ of gold as claimed by the manufacturer) were mixed with 5 mg mL⁻¹ of BSA solution and incubated overnight. Then, solutions were centrifuged and supernatants were discarded. The solid part was redispersed in water to reach an

approximate concentration of 50 mg kg⁻¹ of gold. The exact concentration is not important as it will not affect the migration behavior in the CE. Deionized water (>18 MΩcm⁻¹) from a Milli-Q system (Millipore, Billerica, MA, USA) was used throughout the experiments.

NPs in matrices

The matrix effects on the electrophoretic behavior of NPs were studied by analyzing the surface-coated gold NPs in NOM and FBS solutions. NOM solution was prepared by dissolving SRHA in deionized water to a concentration of 40 mg L⁻¹ of total organic carbon (TOC). The solution was stirred for 24 h in the dark and filtered through 0.2-μm polytetrafluoroethylene membrane filters. NPs with different surface coatings were diluted five times with a matrix solution and allowed to incubate overnight. The final TOC concentration is 5 mg L⁻¹. This concentration is commonly found in a river water system and is also frequently adopted for the investigation of NP aggregation in a NOM matrix [24–26].

Instrumentation

CE separation was performed on a 7100 Capillary Electrophoresis system (Agilent Technology, Santa Clara, CA, USA). Fused-silica capillaries with polyimide external coating (i.d. 50 μm; o.d. 360 μm; length 60 cm) were obtained from Molex (Phoenix, AZ, USA). A new capillary was initialized by flushing with 0.1 N NaOH for 30 min and background electrolyte (BGE) for 30 min, followed by rinsing with water for 5 min. The capillary was conditioned each day before use with 0.1 N NaOH for 15 min, BGE for 15 min, and water for 3 min. Between each run, the capillary was rinsed with water for 60 s and then equilibrated with 0.1 N NaOH and BGE for 3 min, respectively. Samples were hydrodynamically injected at 30 mbar for 15 s followed by an injection of BGE at 15 mbar for 10 s. The temperature of the cartridge was set at 23 °C (ambient temperature), and the applied voltage for the separation was 30 kV. The interface between CE and ICPMS (Agilent 7700x, Agilent Technology, Santa Clara, CA, USA) was set up according to our previously reported method with modifications [27]. Briefly, the outlet of the capillary was directly connected to a Mira Mist CE nebulizer (Burgener Research, Inc., Mississauga, Ontario, Canada). A solution containing 1 % HNO₃ (v/v) was introduced to the nebulizer as a sheath liquid through a platinum tubular electrode by a syringe pump at an infusion rate of 13 μL min⁻¹. An insulated copper wire with a crocodile clip head was used to connect the cathode in CE to the platinum electrode. ICPMS was operated under no gas mode, and mass isotopes ¹⁹⁷Au and ¹¹¹Cd were monitored. Details of the operation conditions are listed in Table 1. The pH value of the BGE was adjusted by adding 1 N NaOH and

Table 1 CE/ICPMS operating parameters

CE parameters	
Capillary	Polymer-coated fused silica capillary, i.d. 50 μm, o.d. 360 μm, length 60 cm
BGE	CHES 10 mM, SDBS 70 mM, pH 10
Makeup solution	1 % HNO ₃ and 10 % 2-propanol in water
Voltage	30 kV
Temperature	23 °C
Sample injection	Hydrodynamic, 30 mbar, 15 s
ICPMS parameters	
RF power	1500 W
Sample depth	8.0 mm
Plasma gas	15.0 L min ⁻¹
Carrier gas flow	1.05 L min ⁻¹
Makeup gas flow	0.50 L min ⁻¹
Monitored isotope	¹⁹⁷ Au, ¹¹¹ Cd
Nebulizer	Mira Mist CE

measured with an Orion Star A214 pH meter (Thermo Scientific, Waltham, MA, USA). Before the analysis, samples were diluted five times with BGE and incubated for 1 h. Then, 5 μL of QD solution was added to the sample vial and 5 s of vortexing was applied to mix the samples. The hydrodynamic sizes were measured with a Malvern Instruments (Worcestershire, UK) Zetasizer Nano ZS dynamic light scattering system. ζ potentials were determined with a Wyatt Technology Möbiuζ light scattering instrument with Dynamics software (Santa Barbara, CA, USA). For simplification, ζ potential values were automatically calculated using the Smoluchowski model for all NPs.

Results and discussion

Surface coating effect

The electrophoretic mobility (μ_{em}) of a particle can be described by the Henry equation [28]

$$\mu_{em} = \frac{\zeta \varepsilon \varepsilon_0}{1.5 \eta} f(\kappa \alpha) \quad (1)$$

where ζ is the zeta potential, ε is the dielectric constant, ε₀ is the permittivity of vacuum, η is the solution viscosity, κ is the Debye parameter, and α is the particle radius. Here, the value of $f(\kappa \alpha)$ varied between 1 and 1.5. Inorganic NPs (gold NP in this case) are commonly coated with a layer of organic molecules to gain colloidal stability in aqueous solution. A wide array of ligand molecules have been developed and identified as useful capping agents for NP stabilization. These molecules varied in sizes (i.e., molecule weight) and bear different functional groups such as carboxyl, amine, and hydroxyl groups,

which, in turn, shape the surface chemistry of NPs. Therefore, NPs with the same core but different surface coating may exhibit a completely different behavior in CE. It should be noted that under current experimental condition, neither Smoluchowski nor Hückel approximation is suitable in describing the nanoparticle investigated in this study [29]. Directly relating experimental parameters to established theory is difficult [30]. Here, we focused our discussion on observed results under varied experimental condition rather than theoretical explanations. Gold NPs with seven different coatings were analyzed by CE under alkali BGE conditions. As shown in Fig. 1, even with the same core size, the migration behaviors are varied significantly among the different coatings.

Relaxation effect of the potential gradient is another factor that can affect the electrophoretic mobility [22]. In this case, differential potential gradients are generating along the sample plug and the rest of capillary filled with running buffer in the initial stage of analysis, and gradually equilibrate with progress of the run. This also causes a run-to-run variation in the calculated electrophoretic mobility and electroosmotic flow. Therefore, polymer-coated QDs were used as an electrophoretic mobility marker to compensate the run-to-run variation of electroosmotic flow (EOF). A QD mobility marker did not cause any effect on electrophoretic mobility and provided concept for the independent calculation of relative electrophoretic mobility in our previous study [21]. Relative electrophoretic mobility (μ_r) is expressed as [21]

$$\begin{aligned}\mu_r &= \mu_{\text{an}} - \mu_{\text{rf}} = (\mu_{\text{an}} + \text{EOF}) - (\mu_{\text{rf}} + \text{EOF}) \\ &= \mu_{\text{an-apparent}} - \mu_{\text{rf-apparent}}\end{aligned}\quad (2)$$

where μ_{an} , $\mu_{\text{an-apparent}}$, μ_{rf} , and $\mu_{\text{rf-apparent}}$ are the electrophoretic mobility and apparent mobility of the analyte (i.e., gold

NPs) and the reference mobility marker (i.e., QDs) respectively. As shown in Figs. 1 and 2a, CA-coated gold NPs of 5, 15, 20, and 30 nm were well separated and their μ_r followed a linear relationship with the size of the particles. Liu and Wei [31] also observed a similar phenomenon and proposed that for separation of gold NPs.

$$\mu_{\text{em}} \propto r \quad (3)$$

When using the relationship described in Eq. (3), surfactant molecules such as sodium dodecyl sulfonate (SDS) are commonly added to the BGE to assist the analysis. Evidences have suggested that the hydrophobic chain of SDS is able to be adsorbed to the gold surface and form a monolayer, which facilitate the separation [31–33]. Because it is difficult to determine the surface charge of a coated NP due to the shielding by the diffuse layer, a ζ potential is commonly serves as an indicator of such property. As shown in Table S2 (see ESM), ζ potential values of CA-coated NPs gradually increased with the size, suggesting that larger NPs carry more negative charges when dispersing in BGE. Our previous studies also confirmed the existence of this relationship, and we further proposed that the surfactant SDBS, an analog of SDS, can interact strongly with gold surface and offer an enhanced size-based separation in CE, compared to a SDS-based system [21]. In addition to the interaction with nanoparticle surface, surfactant molecules can also modify the EOF by altering the BGE viscosity and by interacting with the capillary walls. Therefore, the migration change can be a combined effect of change in the μ_r and EOF. In order to further verify the critical role of SDBS in the separation process and demonstrate the existence of the interaction between surfactant molecules and NPs, we have analyzed gold NPs in the BGE without SDBS while keeping all other conditions unchanged. As shown in

Fig. 1 (a), (b) Electropherogram of gold NPs with different surface coatings. (Separation conditions: SDBS, 70 mM; CHES, 10 mM; pH 10.0; and voltage, 30 kV). Nanoparticles with different surface coatings were individually injected and analyzed by the CE-ICPMS method, and the electropherograms of nanoparticles of different sizes with the same coating material were plotted together in a graph

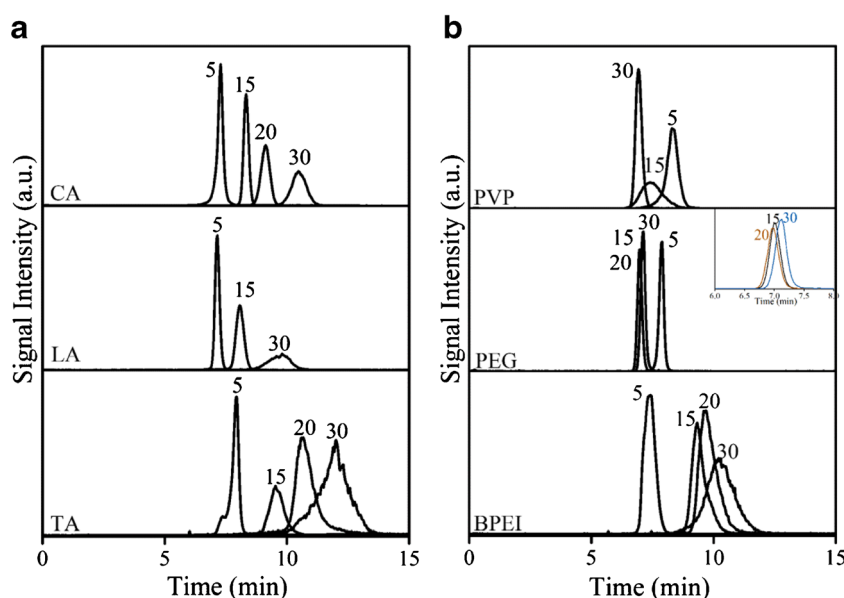


Fig. 2 (a), (b) Surface coating effect on the electrophoretic behavior of surface-coated gold NPs. Relative electrophoretic mobilities were plotted as a function of the diameter

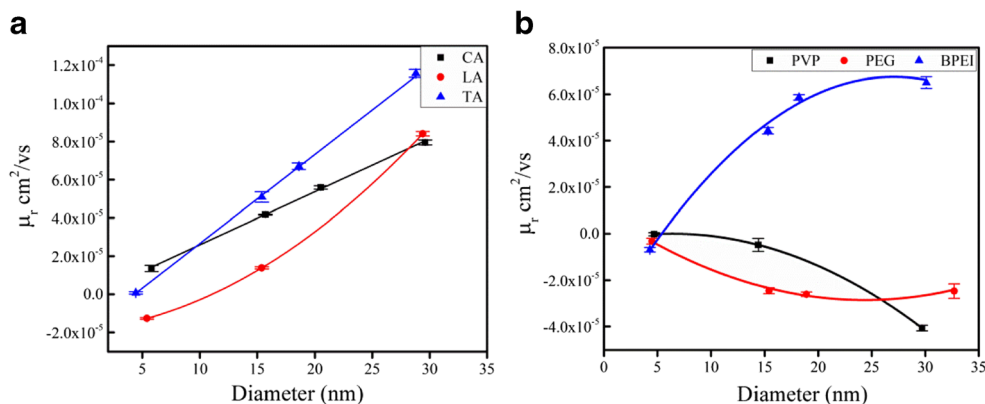


Fig. S1 (see ESM), in the absence of SDBS, gold NPs of different sizes coated with CA presented limited separation. NPs of 15, 20, and 30 nm were almost co-eluted, indicating that CA coating itself was unable to generate enough of a difference in μ_{em} when compared to SDBS which would result in sufficient separation among the different sizes. It should be noted that the ionic strength of the BGE with surfactant is considerably higher than the one without, which also contribute to the change of μ_{em} .

Similar to CA, TA-coated gold NP (Fig. 2a) also demonstrates a linear relationship between particle size and μ_r with good correlation ($R^2 = 0.997$). Both CA and TA rely on the carboxyl groups to be physically adsorbed to the gold NP surface. This type of adsorption is relatively weak, and the ligand can be easily replaced if another type of molecule with stronger interaction with the gold surface is present. The results suggested that the original CA or TA coating can be replaced by SDBS because of the high concentration of SDBS (70 mM) in the BGE and its strong hydrophobic interaction with the gold surface. The critical micelle concentration value of SDBS is 1.28 mM [34]. However, it is noticed that the slope values of the correlation for CA and TA are different, suggesting that the magnitude of ligand replacement is different. Although it is difficult to determine the exact surface coverage of SDBS on a gold NP surface, we believe that the bulkiness of TA, hydrophobic nature of the aromatic ring structure, and its multiple interactions with the gold surface molecule may hamper the ligand exchange process, resulting in a different surface composition from CA-coated gold NP. For LA coating (Fig. 2a), the ligand molecules are attached to the gold surface through a covalent S–Au bond. In this case, surfactant molecules interact with the LA ligand layer instead of directly replacing the original coating, which contributed to the non-linear correlation profile. It is worth mentioning that the ζ potential values of both TA- and LA-coated NPs followed a similar trend to CA-coated NPs, which further support relationship described in Eq. (3).

For NP stabilization, polymer-based ligand molecules are usually preferred over small molecules because they can offer

stronger ligand-particle interaction due to their multi-dentate style of binding. Additionally, the polymer layer can provide steric repulsion which further enhances nanoparticle stability in different dispersing conditions. From Fig. 2b, it is very clear that polymer-coated gold NPs presented a completely different set of behaviors in CE than did small molecules. For PVP- and PEG-coated particles, μ_r has negative values, indicating that these NPs moved slower than the mobility markers during the analysis. It should be noted here that because both mobility marker, i.e., QDs with carboxyl group, and gold NPs coated with PVP and PEG carry a negative charge under the current BGE conditions (pH = 10), all NPs in the capillary, including QDs, should have an μ_{em} towards the anode side. Therefore, the results indicated that larger particles with a PEG or PVP coating showed a smaller magnitude of μ_{em} than the smaller particle with the same coating. Both PEG and PVP coatings only render limited negative surface charges to the NPs, and the polymer layer may also limit the attachment or adsorption of SDBS to the NP surface. We proposed that the assumption that NPs with larger diameter carry more surface charge because of the increased surface area for ligand molecules may not be viable under this circumstance. The results from ζ potential measurement (ESM Table S2) confirmed our theory, where gold NPs coated with PVP and PEG exhibited very small changes among the different sizes. Consequently, other factors such as the diameter of the NP may have a stronger influence on the μ_{em} for PEG- and PVP-coated NPs when dispersed in the SDBS containing BGE. It is interesting that NPs coated with cationic BPEI polymer display similar behaviors to the ones coated with small negatively charge ligands. BPEI contains numerous amine groups and is strongly positively charged in aqueous solution at neutral pH. Under a strong alkali condition, amine groups are deprotonated and the surface charge is minimized which can cause reduction in separation among the different sizes. As shown in Fig. S2 (see ESM), the results agreed with our assumption that without adding SDBS, BPEI-coated NPs were poorly separated. When SDBS was added, μ_r followed an almost linear relationship from 5 to 20 nm with the size of the NPs. The ζ potential

values also increased gradually with the particle sizes from 5 to 20 nm and exhibited only a small change when NP size was further grown to 30 nm. This result suggested that there was a strong interaction between the SDBS and BPEI coating, which allowed the surfactant to mask the original surface charges. The linearity of the correlation was not extended to 30 nm, which can be attributed to the insufficient increase in the negative surface charge arising from SDBS compared to the growth of the NP size.

Many studies have reported the formation of a protein corona on the gold NP surface and suggested the adsorption can be very stable due to multi-point interactions or the exposed thiol group of the cysteine residue [35–37]. We selected BSA to study the migration behavior of gold NP with a protein coating. As shown in Fig. 3, the μ_r values were negative and very close for all sizes in this study. Proteins are known to carry both positively and negatively charged functional groups such as carboxyl and amine groups. The results suggest that when the protein corona is formed, the migration of the particle is largely based on the migration of the adsorbed proteins, such that changes in the diameter of the particle have no significant impact on the mobility.

Matrix effect

The matrix effect on the electrophoretic behavior of NP in the capillary electrophoresis is studied by analyzing the surface-coated NPs in the river water simulant and serum. With the growing use of nanotechnology in manufacturing processes of consumer products, there is a sharp increase in the release of nanomaterials to the environment. Carefully characterizing the nanomaterials will assist in the study of their transport, fate, and impact on the environment. DLS was used to monitor the colloidal stability before and after incubation of NP in the NOM matrix. It has been reported that the NOM can be

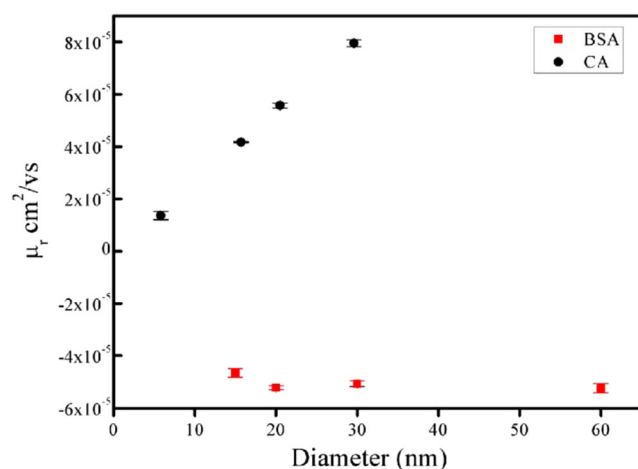


Fig. 3 Relative electrophoretic mobility as a function of the diameter of gold NP with BSA coating

adsorbed to the surface of NPs and influences their stability. From ESM Table S1, NPs of all sizes with varied surface coating in this study showed an increase in the hydrodynamic size which can be attributed to the adsorption of NOM to the NP surface. Stankus and coworkers reported that NOM is able to interact with gold NPs regardless of the capping agents, even for PVP, which is a type of ligand that is frequently used to render strong colloidal stability of NPs [24]. The increases of hydrodynamic size for 15-, 20-, and 30-nm gold NP are relatively small, suggesting that the magnitude of the interaction is limited. For 5 nm, however, the change is more significant compared to bigger particles. This can be explained by the higher surface curvature of very small particle, which restricts the surface coverage of capping ligand resulting in less resistance to the adsorption of NOM. Nonetheless, no aggregation was observed for NP dispersed in the NOM matrix. Samples were then analyzed by CE-ICPMS. From the electropherogram (Fig. 4a, b), gold NPs that are capped with small ligand molecules including CA and TA exhibited a marginal decrease in the μ_r compared to the one with water as a matrix while the change was negligible for LA-capped NPs (Fig. 4c), suggesting that the NOM matrix did not significantly interfere with the CE analysis. Our study also indicated that SDBS, an analog of SDS, can interact strongly with gold surface and offer an enhanced size-based separation in CE compared to a SDS-based system. Therefore, it is reasonable to believe that for gold NPs that are stabilized with small ligands, the SDBS surfactant in the BGE is either able to directly replace (in the case of ligands that rely on physisorption such as carboxyl groups of CA and TA) or interact (LA-coated NP) with the coating, which effectively masks or eliminates the adsorption of NOM. For polymer coatings, the effect of NOM was not obvious on PEG- and PVP-coated NPs (Fig. 4d, e), as evidenced by the small changes in the μ_r . A stronger matrix effect of NOM can be observed in samples with BPEI coatings where μ_r of all sizes exhibited a decrease with similar magnitude (Fig. 4f). This can be attributed to the adsorption of NOM to the BPEI coating, which interferes with the anchoring of the SDBS surfactant to the NP surface.

The matrix effects related to the adsorption of biological molecules on the migration of surface-coated gold NPs in CE were studied. FBS is an excellent candidate for the investigation because it contains not only a wide array of chemical substances, including proteins, electrolytes, and hormones, but it also has very high ionic strength which can be detrimental to NP stability. DLS was first used to monitor if any aggregation occurred after dispersing gold NP in the serum. As suggested by the results in ESM Table S1, for all six different coatings, there was no detectable aggregation. Because FBS contains a variety of proteins and antibodies, it is expected that these molecules in the serum can replace weakly adsorbed ligand such as CA and TA. From the electropherogram (Fig. 5), we see a drastic change in the migration behavior as

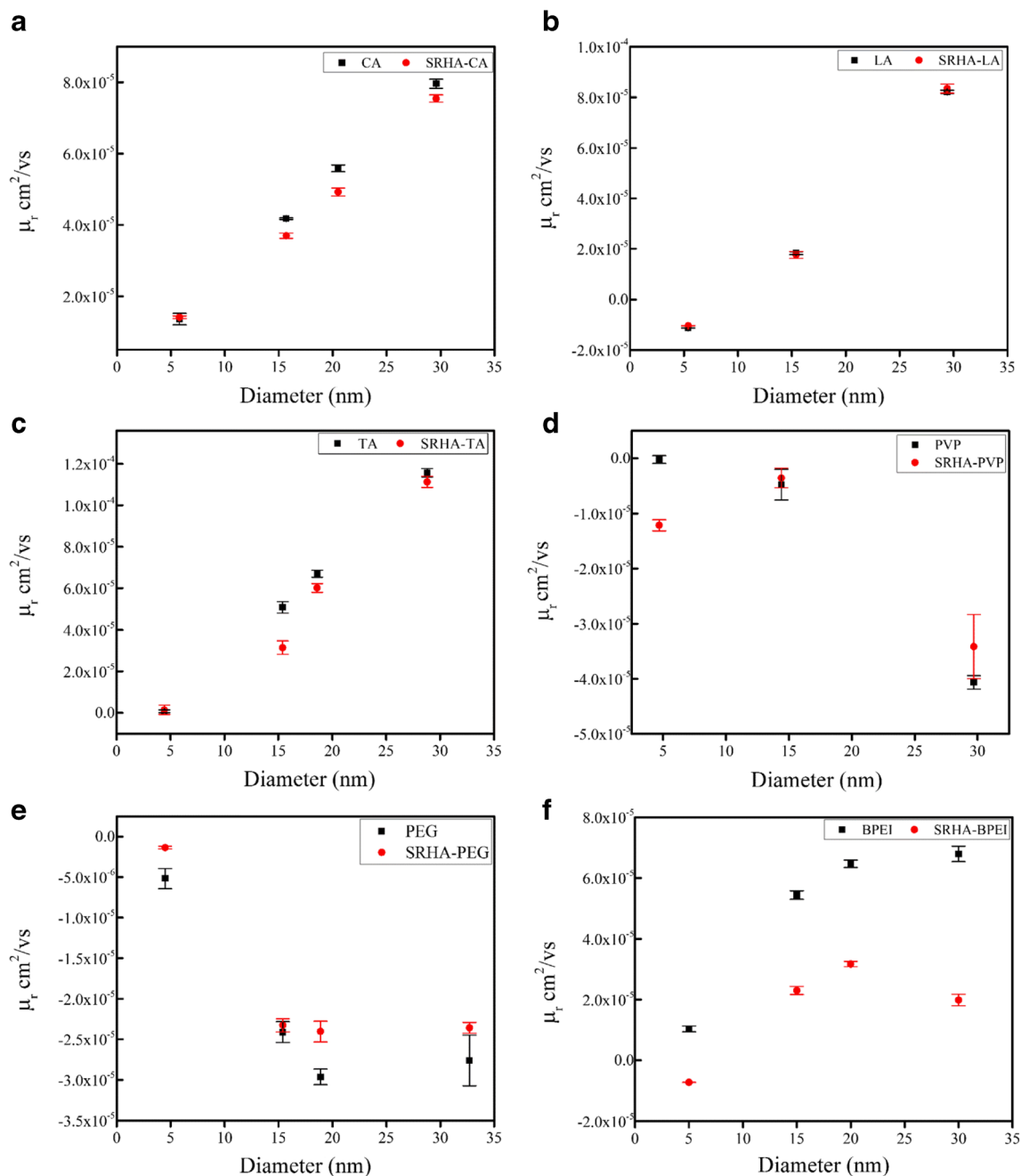


Fig. 4 (a)–(f) NOM matrix effect on the electrophoretic behavior of surface-coated gold NPs. The relative electrophoretic mobilities in water (*black square*) and SRHA solution (*red circle*) are plotted as a function of the diameter

compared to the NPs with the original coating. For the small ligand-coated NPs (CA, LA, and TA), μ_r of all coatings had very similar values and only showed a small fluctuation for the entire size range. It is worth mentioning that this behavior was very similar to the results observed for BSA-coated NPs, suggesting that protein molecules covered a significant portion of the NP surface. Compared to small ligand coatings, polymer coatings usually offer higher stability. As shown in the electropherogram, PVP and BPEI coatings did not present a strong resistance to the matrix component in FBS, and the

correlation between the size and μ_r for the original coatings diminished. For PEG coating, the values of μ_r for 15, 20, and 30 nm in FBS are almost the same as the NPs in water solution. The results agreed with the literature reports that PEG is effective in enhancing the blood circulation time of nanomaterials by reducing protein-particle interactions. NPs of 5 nm with PEG coating, however, exhibited a different μ_r value. This could be attributed to the large surface curvature of small NP, which resulted in insufficient protection from the ligand and increased particle-matrix interaction.

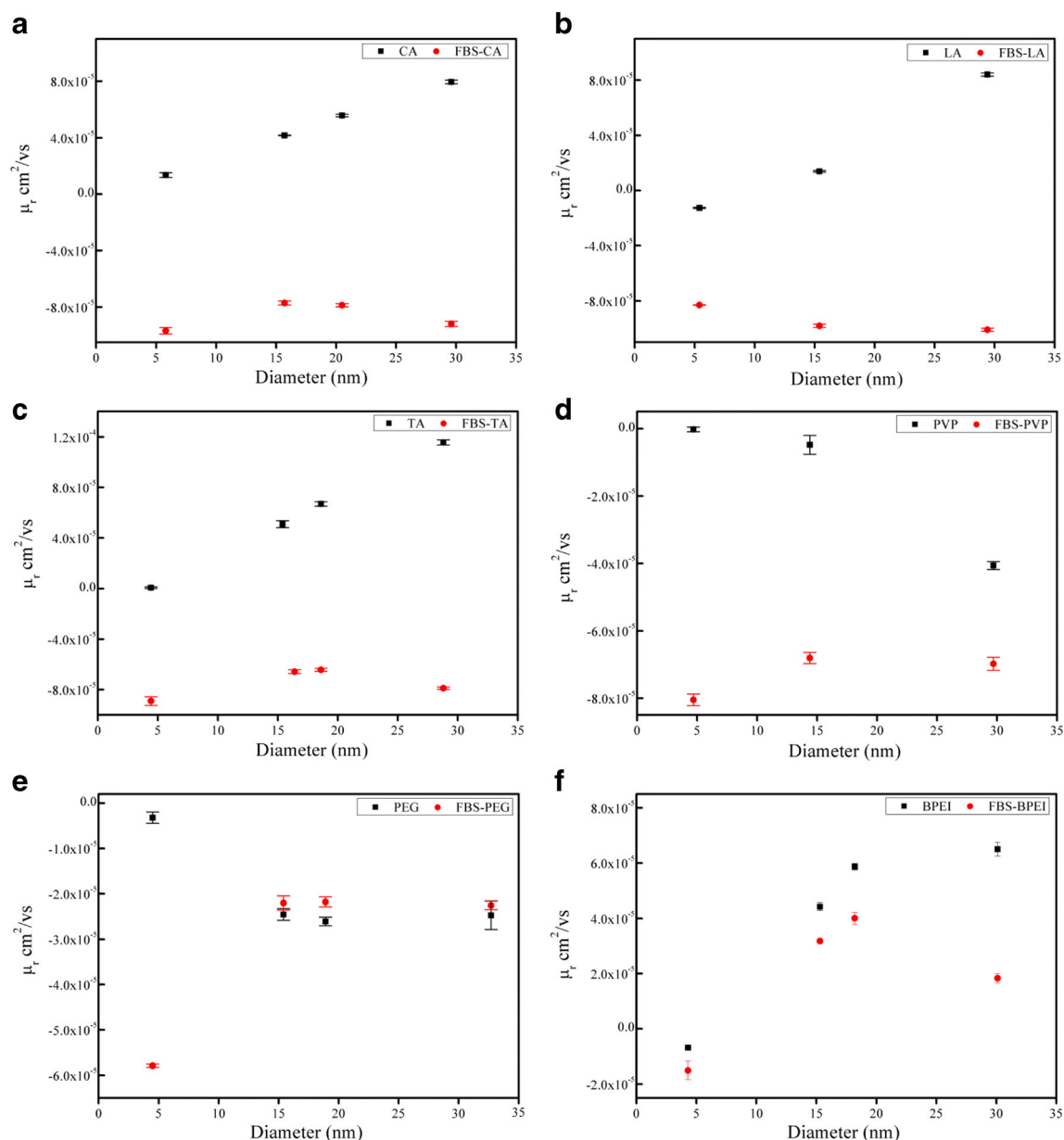


Fig. 5 (a)–(f) FBS matrix effect on the electrophoretic behavior of surface-coated gold NPs. The relative electrophoretic mobilities are plotted as a function of the diameter of gold NP

Conclusion

We have performed a systematic study to investigate the electrophoretic behavior of gold NPs in CE. The results suggested that there was strong interaction between the surfactant molecules and the NPs. The magnitude and effect of the interaction, however, is highly dependent on the surface composition of the NPs. The μ_r of NPs with small molecules as ligand in this study were positively correlated with NP diameter, and the correlations are linear for CA and TA coatings. Negative correlation was found for PVP and PEG coatings which can be attributed to the limited surface charge offered by these two ligands. The cationic polymer BPEI exhibited similar migration behavior as

CA- and TA-coated NPs, suggesting SDBS interacts with the coating and masks the original charge. For BSA coating, the results indicated that a protein corona was formed on the gold surface, minimizing the difference in charge-to-size ratio among samples, which resulted in a small fluctuation in μ_r for the sizes being studied. For environmental matrix effect, the NOM in the SRHA solution did not largely alter the migration behavior of gold NP. It can be explained by the strong adsorption of SDBS to the particle surface which effectively reduced the influence of NOM. However, the surfactant was unable to eliminate the matrix effects associated with a complex biological matrix like serum. The correlation μ_r with NP size in the serum is similar to gold NPs with BSA coating, indicating that

protein molecules adsorbed to the gold surface and masked the characteristics of the original coating. The results from this study highlighted the necessity to establish size calibration by using surface coating and matrix-matched standards to obtain accurate size-based characterization for unknown samples. Further development is underway to evaluate the possibility of simplifying the method which allows for the use of reduced numbers of standards to generate a generalized calibration for multiple NPs.

Acknowledgments These studies were conducted using the Nanotechnology Core Facility (NanoCore) located on the US Food and Drug Administration's Jefferson Laboratories campus (Jefferson, AR), which houses the FDA National Center for Toxicological Research and the FDA Office of Regulatory Affairs/Arkansas Regional Laboratory. We thank Patrick Sisco, Crystal Ford, Jin-Hee Lim, Yasith Nanayakkara, Venu Gopal Bairi, and Nuwan Kothalawala for their valuable comments on the draft manuscript. This project was supported in part by an appointment to the Research Participation Program at the Office of Regulatory Affairs/Arkansas Regional Laboratory, US Food and Drug Administration, administered by the Oak Ridge Institute for Science and Education through an interagency agreement between the US Department of Energy and FDA. The views expressed in this document are those of the authors and should not be interpreted as the official opinion or policy of the US Food and Drug Administration, Department of Health and Human Services, or any other agency or component of the US government. The mention of trade names, commercial products, or organizations is for clarification of the methods used and should not be interpreted as an endorsement of a product or manufacturer.

Compliance with ethical standards

Conflict of interest The authors declare that they have no conflict of interest.

References

1. Stebounova LV, Morgan H, Grassian VH, Brenner S. Health and safety implications of occupational exposure to engineered nanomaterials. *Wiley Interdiscip Rev Nanomed Nanobiotechnol*. 2012;4(3):310–21.
2. Nyström AM, Fadeel B. Safety assessment of nanomaterials: implications for nanomedicine. *J Control Release*. 2012;161(2):403–8.
3. Dhawan A, Sharma V. Toxicity assessment of nanomaterials: methods and challenges. *Anal Bioanal Chem*. 2010;398(2):589–605.
4. Chithrani BD, Ghazani AA, Chan WCW. Determining the size and shape dependence of gold nanoparticle uptake into mammalian cells. *Nano Lett*. 2006;6(4):662–8.
5. Lewinski N, Colvin V, Drezek R. Cytotoxicity of nanoparticles. *Small*. 2008;4(1):26–49.
6. Calzolari L, Gilliland D, Rossi F. Measuring nanoparticles size distribution in food and consumer products: a review. *Food Addit Contam Part A*. 2012;29(8):1183–93.
7. von der Kammer F, Ferguson PL, Holden PA, Masion A, Rogers KR, Klaine SJ, et al. Analysis of engineered nanomaterials in complex matrices (environment and biota): general considerations and conceptual case studies. *Environ Toxicol Chem*. 2012;31(1):32–49.
8. Jenkins SV, Qu H, Mudalige T, Ingle TM, Wang R, Wang F, et al. Rapid determination of plasmonic nanoparticle agglomeration status in blood. *Biomaterials*. 2015;51:226–37.
9. Anderson W, Kozak D, Coleman VA, Jämting ÅK, Trau M. A comparative study of submicron particle sizing platforms: accuracy, precision and resolution analysis of polydisperse particle size distributions. *J Colloid Interface Sci*. 2013;405:322–30.
10. Zhou X-X, Liu R, Liu J-F. Rapid chromatographic separation of dissoluble Ag(I) and silver-containing nanoparticles of 1–100 nanometer in antibacterial products and environmental waters. *Environ Sci Technol*. 2014;48(24):14516–24.
11. Soto-Alvaredo J, Montes-Bayón M, Bettmer J. Speciation of silver nanoparticles and silver(I) by reversed-phase liquid chromatography coupled to ICPMS. *Anal Chem*. 2013;85(3):1316–21. doi:10.1021/ac302851d.
12. Mudalige TK, Qu H, Linder SW. Asymmetric flow-field flow fractionation hyphenated ICP-MS as an alternative to cloud point extraction for quantification of silver nanoparticles and silver speciation: application for nanoparticles with a protein corona. *Anal Chem*. 2015;87(14):7395–401.
13. Qu H, Mudalige TK, Linder SW. Capillary electrophoresis coupled with inductively coupled mass spectrometry as an alternative to cloud point extraction based methods for rapid quantification of silver ions and surface coated silver nanoparticles. *J Chromatogr A*. 2016;1429:348–53.
14. Schmidt B, Loeschner K, Hadrup N, Mortensen A, Sloth JJ, Bender Koch C, et al. Quantitative characterization of gold nanoparticles by field-flow fractionation coupled online with light scattering detection and inductively coupled plasma mass spectrometry. *Anal Chem*. 2011;83(7):2461–8.
15. Mudalige TK, Qu H, Linder SW. An improved methodology of asymmetric flow field flow fractionation hyphenated with inductively coupled mass spectrometry for the determination of size distribution of gold nanoparticles in dietary supplements. *J Chromatogr A*. 2015;1420:92–7.
16. Gray EP, Bruton TA, Higgins CP, Halden RU, Westerhoff P, Ranville JF. Analysis of gold nanoparticle mixtures: a comparison of hydrodynamic chromatography (HDC) and asymmetrical flow field-flow fractionation (AF4) coupled to ICP-MS. *J Anal At Spectrom*. 2012;27(9):1532–9.
17. Giddings JC. Field-flow fractionation: analysis of macromolecular, colloidal, and particulate materials. *Science*. 1993;260(5113):1456–65.
18. Wahlund K-G. Flow field-flow fractionation: critical overview. *J Chromatogr A*. 2013;1287:97–112.
19. Gigault J, Pettibone JM, Schmitt C, Hackley VA. Rational strategy for characterization of nanoscale particles by asymmetric-flow field flow fractionation: a tutorial. *Anal Chim Acta*. 2014;809:9–24.
20. Gigault J, Hackley VA. Observation of size-independent effects in nanoparticle retention behavior during asymmetric-flow field-flow fractionation. *Anal Bioanal Chem*. 2013;405(19):6251–8.
21. Qu H, Mudalige TK, Linder SW. Capillary electrophoresis/inductively-coupled plasma-mass spectrometry: development and optimization of a high resolution analytical tool for the size-based characterization of nanomaterials in dietary supplements. *Anal Chem*. 2014;86(23):11620–7.
22. Ikuta N, Sakamoto H, Yamada Y, Hirokawa T. Numerical simulation for capillary electrophoresis: II. Relaxation effect of potential gradient in capillary zone electrophoresis. *J Chromatogr A*. 1999;838(1–2):19–29.
23. Martin MN, Allen AJ, MacCuspie RI, Hackley VA. Dissolution, agglomerate morphology, and stability limits of protein-coated silver nanoparticles. *Langmuir*. 2014;30(38):11442–52.
24. Stankus DP, Lohse SE, Hutchison JE, Nason JA. Interactions between natural organic matter and gold nanoparticles stabilized with

- different organic capping agents. *Environ Sci Technol.* 2011;45(8):3238–44.
25. Li X, Lenhart JJ. Aggregation and dissolution of silver nanoparticles in natural surface water. *Environ Sci Technol.* 2012;46(10):5378–86.
 26. Louie SM, Spielman-Sun ER, Small MJ, Tilton RD, Lowry GV. Correlation of the physicochemical properties of natural organic matter samples from different sources to their effects on gold nanoparticle aggregation in monovalent electrolyte. *Environ Sci Technol.* 2015;49(4):2188–98.
 27. Qu H, Mudalige TK, Linder SW. Arsenic speciation in rice by capillary electrophoresis/inductively coupled plasma mass spectrometry: enzyme-assisted water-phase microwave digestion. *J Agric Food Chem.* 2015;63(12):3153–60.
 28. Henry DC. The cataphoresis of suspended particles. Part I. *Equ Cataphoresis Proc Roy Soc A.* 1931;133(821):106–29.
 29. Doane TL, Chuang C-H, Hill RJ, Burda C. Nanoparticle ζ -potentials. *Acc Chem Res.* 2012;45(3):317–26.
 30. Schnabel U, Fischer C-H, Kenndler E. Characterization of colloidal gold nanoparticles according to size by capillary zone electrophoresis. *J Microcolumn Sep.* 1997;9(7):529–34.
 31. Liu FK, Wei GT. Adding sodium dodecylsulfate to the running electrolyte enhances the separation of gold nanoparticles by capillary electrophoresis. *Anal Chim Acta.* 2004;510(1):77–83.
 32. Soares DM, Gomes WE, Tenan MA. Sodium dodecyl sulfate adsorbed monolayers on gold electrodes. *Langmuir.* 2007;23(8):4383–8.
 33. Burgess I, Jeffrey CA, Cai X, Szymanski G, Galus Z, Lipkowski J. Direct visualization of the potential-controlled transformation of hemimicellar aggregates of dodecyl sulfate into a condensed monolayer at the Au(111) electrode surface. *Langmuir.* 1999;15(8):2607–16.
 34. Chauhan S, Sharma K. Effect of temperature and additives on the critical micelle concentration and thermodynamics of micelle formation of sodium dodecyl benzene sulfonate and dodecyltrimethylammonium bromide in aqueous solution: a conductometric study. *J Chem Thermodyn.* 2014;71:205–11.
 35. Tsai D-H, DelRio FW, Keene AM, Tyner KM, MacCuspie RI, Cho TJ, et al. Adsorption and conformation of serum albumin protein on gold nanoparticles investigated using dimensional measurements and in situ spectroscopic methods. *Langmuir.* 2011;27(6):2464–77.
 36. Brewer SH, Glomm WR, Johnson MC, Knag MK, Franzen S. Probing BSA binding to citrate-coated gold nanoparticles and surfaces. *Langmuir.* 2005;21(20):9303–7.
 37. Prapainop K, Witter DP, Wentworth P. A chemical approach for cell-specific targeting of nanomaterials: small-molecule-initiated misfolding of nanoparticle corona proteins. *J Am Chem Soc.* 2012;134(9):4100–3.